Original Manuscript

Progress in Reaction Kinetics and Mechanism

Progress in Reaction Kinetics
and Mechanism
Volume 47: 1–18

DOI: 10.1177/14686783221090374
journals.sagepub.com/home/prk
SAGE

Melting aspects in flow of second grade nanomaterial with homogeneous–heterogeneous reactions and irreversibility phenomenon: A residual error analysis

Faris Alzahrani[1] and Muhammad Ijaz Khan[1,2]

Abstract

Here, we scrutinize the entropy analysis in magnetohydrodynamic flow of second-grade nanomaterials with melting effect subject to stretchable bended surface. Heat attribution is modeled through first law of thermodynamics with radiation effect. Major physical effect of random and thermophoretic motion is also addressed. Feature of irreversibility (entropy rate) analysis is also discussed. Isothermal cubic autocatalyses chemical reaction at catalytic surface is discussed. Nonlinear dimensionless differential system is developed through adequate transformation. Optimal homeotypic analysis method (OHAM) is employed to construct convergent solution. Influence of physical variables on entropy rate, fluid flow, concentration, and thermal field is discussed. An augmentation in fluid flow is noticed through curvature variable, while reverse effect holds for magnetic variable. A reverse effect holds for fluid flow and thermal field through melting variable. Entropy analysis is augmented with variation in melting variable. Reduction occurs in concentration through thermophoretic variable, while an opposite effect holds for thermal field. An increment in melting variable leads to reduced concentration. Larger estimation of radiation variable improves entropy analysis.

[1]Nonlinear Analysis and Applied Mathematics (NAAM)-Research Group, Department of Mathematics, Faculty of Sciences, King Abdulaziz University, Jeddah, Saudi Arabia
[2]Department of Mathematics and Statistics, Riphah International University I-14, Islamabad, Pakistan

Corresponding author:
M Ijaz Khan, Department of Mathematics and Statistics, Riphah International University I-14, Islamabad 44000, Pakistan.
Email: mikhan@math.qau.edu.pk

Keywords
Second-grade fluid, curved stretching surface, melting heat, thermal radiation, brownian diffusion thermophoresis, entropy generation, heat generation/absorption and homogeneous and heterogeneous chemical reactions

Introduction

It is known fact that melting phenomenon plays a vital role in various industrial and engineering applications. Melting phenomenon is sufficiently utilized in welding process, heat engines, permafrost melting, semiconductor material processing, coil exchangers, magma solidification, and many others. Melting phenomenon was first studied by Robert.[1] He considered a slab of ice and investigated its melting process when in contact with hot stream air. Hayat et al.[2] explored the effects of melting heat transfer in magnetohydrodynamic non-Newtonian Oldroyd-B fluid with variable thickness due to stretching surface. They achieved convergent series solutions by utilizing homotopic technique. Das[3] considered thermal radiation effects while exploring melting phenomenon in magnetohydrodynamic boundary layer flow due to moving surface. Khan et al.[4] discussed the melting effect in dissipative flow of nanomaterials with entropy analysis toward a stretchable surface. Further investigations of melting phenomenon are illustrated in Refs.[5–10]

Fluids as carriers are used in a variety of heat transfer equipment. The efficiency of these devices can be improved by enhancing the thermal conductivity of fluids. It is done by adding small nanosize particles in base fluid. This idea was initially revealed by Choi et al.[11,12] Due to superior thermal properties, nanofluids have numerous applications in heat transfer related devices, boiling heat transfer, solar thermal systems, convective heat transfer as well as condensation and evaporation.[13] Nanofluids with stable suspension of nanoparticles in base fluid have a great prospect to meet the modern requirements of innovative thermal, industrial, and cooling technology.[14] Buongiorno[15] gives accomplished advanced concept on nanomaterials heat conduction augmentation. A comprehensive analysis on challenges, opportunities, synthesis, and stability of nanofluids is performed by Urmia et al.[16] Reddy and Makinde[17] examined buoyancy forces, thermophoretic, and Brownian motion for magnetohydrodynamic nanofluid flow in an asymmetric channel. Nonlinear mixed convection, thermo diffusion, and diffusion thermo effects in nanofluid flow are addressed by Hayat et al.[18] Irreversibility analysis in radiative flow of second-grade nanomaterials with Lorentz force and radiation effect subject to stretched sheet is performed by Hayat et al.[19] Some recent developments in nanofluids are given in Refs.[20–25]

Entropy generation is used to determine the performance of various isolated thermal systems in manufacturing, engineering, refrigerators, thermal transportation phenomenon, hybrid-powered engines, industrial, and various biological processes. Entropy production occurs due to fluids friction, Joule heating, diffusion, friction of solid surfaces, electric resistance, molecules vibration, unstained expansion chemical reaction, thermal resistance to the liquid flow, etc. Entropy minimization is used to augments of any thermal system performance. Bejan[26,27] gives the concept of entropy minimization in convective fluid flow. Kumar et al.[28] discussed irreversibility investigation in magnetohydrodynamic incompressible flow of Williamson nanoliquid. Irreversibility in reactive magnetohydrodynamic couple stress liquid flow through a saturated permeable channel is illustrated by Hassan.[29] Few recent investigations about irreversibility (entropy rate) analysis are highlighted in Refs.[30–40]

Motivated from above-mentioned studies and the numerous industrials applications of the recent problem, it is main interest in this exploration to discuss the melting effect in hydromagnetic flow of second-grade nanofluid with entropy analysis by a stretchable curved surface. Heat equation is scrutinized through first law of thermodynamics with radiation effect. Random and thermophoresis

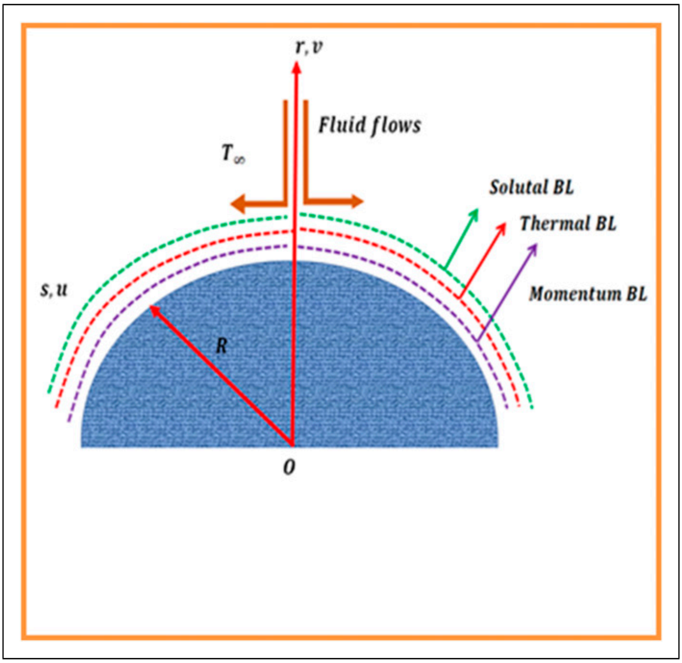

Figure 1. Flow sketch.

motion are considered. Features of entropy generation are addressed. Homogeneous–heterogeneous chemical reactions are considered at catalytic surface. By employing similarity variables, we get dimensionless ordinary differential system. Optimal homotopic analysis technique (OHAM) is implemented to develop convergent solution.[41–45] Influence of fluid flow, entropy generation, thermal field, and concentration against physical parameters are graphically discussed.

Statement

Two-dimensional hydromagnetic flow of an incompressible second-grade nanomaterial with melting effect is addressed. Heat equation is developed through first law of thermodynamics with thermal radiation. Brownian motion and thermophoretic effects are considered. Entropy features are also considered. Furthermore, homogeneous–heterogeneous chemical reactions are considered at catalytic surface. Magnetic force of strength (B_0) is implemented. Suppose that $u_w = as$ the stretching velocity with rate constant $(a > 0)$. Figure 1 shows the physical flow diagram.

Isothermal cubic autocatalytic reactions satisfy[46–49]

$$A + 3B \rightarrow 4B, \qquad \text{with reaction rate} = k_1^* C_2 C_2^2 \tag{1}$$

First-order chemical reaction is given as

$$A \rightarrow B, \qquad \text{with reaction rate} = k_2^* C_2 \tag{2}$$

Under above assumption, the governing equation becomes[50–52]

$$(r + R)\frac{\partial v}{\partial r} + v + R\frac{\partial u}{\partial s} = 0, \tag{3}$$

$$\frac{u^2}{r+R}+\frac{1}{\rho_f}\frac{\partial p}{\partial r}=0, \tag{4}$$

$$\left.\begin{aligned}
&v\frac{\partial u}{\partial r}+\frac{uR}{r+R}\frac{\partial u}{\partial s}+\frac{uv}{r+R}=-\frac{1}{\rho_f}\frac{R}{r+R}\frac{\partial p}{\partial s}+\nu_f\left(\frac{\partial^2 u}{\partial r^2}+\frac{1}{(r+R)}\frac{\partial u}{\partial r}-\frac{u}{(r+R)^2}\right)\\
&+\frac{\alpha_1^*}{\rho_f}\left(\begin{array}{l}\frac{2R}{(r+R)}\frac{\partial^2 u}{\partial r^2}\frac{\partial u}{\partial s}-\frac{2R}{(r+R)^2}\frac{\partial u}{\partial r}\frac{\partial u}{\partial s}+\frac{2}{(r+R)}\frac{\partial v}{\partial r}\frac{\partial u}{\partial r}+\frac{2}{(r+R)}v\frac{\partial^2 u}{\partial r^2}\\ -\frac{2}{(r+R)}v\frac{\partial u}{\partial r}-\frac{4R}{(r+R)^2}u\frac{\partial^2 u}{\partial r\partial s}-\frac{4R}{(r+R)^2}u\frac{\partial v}{\partial r}+\frac{2R}{(r+R)^3}u\frac{\partial u}{\partial s}\end{array}\right)-\frac{\sigma_f}{\rho_f}B_0^2 u
\end{aligned}\right\}, \tag{5}$$

$$\left.\begin{aligned}
&v\frac{\partial T}{\partial r}+\frac{uR}{r+R}\frac{\partial T}{\partial s}=\left(\frac{k}{(\rho c_p)_f}+\frac{16\sigma^* T_\infty^3}{3k^*(\rho c_p)_f}\right)\left(\frac{1}{r+R}\frac{\partial T}{\partial r}+\frac{\partial^2 T}{\partial r^2}\right)\\
&+\tau\left(D_{C_1}\frac{\partial C_1}{\partial r}\frac{\partial T}{\partial r}+\frac{D_T}{T_\infty}\left(\frac{\partial T}{\partial r}\right)^2+D_{C_2}\frac{\partial C_2}{\partial r}\frac{\partial T}{\partial r}\right)+\frac{Q_0}{(\rho c_p)_f}(T-T_\infty)
\end{aligned}\right\}, \tag{6}$$

$$v\frac{\partial C_1}{\partial r}+\frac{uR}{r+R}\frac{\partial C_1}{\partial s}=D_{C_1}\left(\frac{1}{r+R}\frac{\partial C_1}{\partial r}+\frac{\partial^2 C_1}{\partial r^2}\right)+\frac{D_T}{T_\infty}\left(\frac{1}{r+R}\frac{\partial T}{\partial r}+\frac{\partial^2 T}{\partial r^2}\right)-k_1^* C_1 C_2^2, \tag{7}$$

$$v\frac{\partial C_2}{\partial r}+\frac{uR}{r+R}\frac{\partial C_2}{\partial s}=D_{C_2}\left(\frac{1}{r+R}\frac{\partial C_2}{\partial r}+\frac{\partial^2 C_2}{\partial r^2}\right)+\frac{D_T}{T_\infty}\left(\frac{1}{r+R}\frac{\partial T}{\partial r}+\frac{\partial^2 T}{\partial r^2}\right)+k_1^* C_1 C_2^2, \tag{8}$$

$$\left.\begin{aligned}
&u=as,\ \ T=T_m,\ \ D_{C_1}\frac{\partial C_1}{\partial r}=-D_{C_2}\frac{\partial C_2}{\partial r}=k_2^* C_1\ \text{at}\ r=0,\\
&u\to 0,\ \ \frac{\partial u}{\partial r}\to 0,\ \ T\to T_\infty,\ \ C_1\to C_0,\ C_2\to 0\ \ \text{as}\ \ r\to\infty.\\
&k_f\left(\frac{\partial T}{\partial r}\right)=\rho_f[\lambda+C_s(T_m-T_0)]v(s,0)
\end{aligned}\right\}. \tag{9}$$

By using

$$\left.\begin{aligned}
&u=asf'(\eta),\ \ v=-\frac{R}{r+R}\sqrt{a\nu_f}f(\eta),\ \ p=\rho_f a^2 s^2 P(\eta),\\
&\theta(\eta)=\frac{T-T_m}{T_\infty-T_m},\ \ \varphi(\eta)=\frac{C_1}{C_0},\ \ l(\eta)=\frac{C_2}{C_0},\eta=\sqrt{\frac{a}{\nu_f}}r,
\end{aligned}\right\} \tag{10}$$

we have

$$P'-\frac{f'^2}{(\eta+K)}=0, \tag{11}$$

$$\left.\begin{array}{l}\frac{2A}{(\eta+K)}P=f'''+\frac{1}{(\eta+K)}f''-\frac{1}{(\eta+K)^2}f'+\frac{K}{(\eta+K)}ff''+\frac{K}{(\eta+K)^2}ff'-\frac{K}{(\eta+K)}f'^2\\ \beta\left(\frac{2K}{(\eta+K)}f'f'''-\frac{2K}{(\eta+K)^2}ff'''-\frac{8K}{(\eta+K)^2}f'f''+\frac{4K}{(\eta+K)^3}ff''+\frac{6K}{(\eta+K)^3}f'^2-\frac{4K}{(\eta+K)^4}ff'\right)-Mf',\end{array}\right\} \tag{12}$$

$$(1+Rd)\left(\theta''+\frac{1}{(\eta+K)}\theta'\right)+\mathrm{Pr}\frac{A}{(\eta+K)}f\theta'+\mathrm{Pr}Nt\theta'^2+\mathrm{Pr}Q\theta=0, \tag{13}$$

$$\frac{1}{Sc}\left(\varphi''+\frac{1}{(\eta+K)}\varphi'\right)+\frac{K}{(\eta+K)}f\varphi'+\frac{1}{Sc}\frac{Nt}{Nb}\left(\theta''+\frac{1}{(\eta+K)}\theta'\right)-K_1\varphi l^2=0, \tag{14}$$

$$\frac{\delta}{Sc}\left(l''+\frac{1}{(\eta+K)}l'\right)+\frac{K}{(\eta+K)}fl'+\frac{1}{Sc}\frac{Nt}{Nb}\left(\theta''+\frac{1}{(\eta+K)}\theta'\right)+K_1\varphi l^2=0, \tag{15}$$

with

$$\left.\begin{array}{c}f'(\eta)=1,\ \theta(\eta)=0,\ \ \mathrm{Pr}f(\eta)+Me\theta'(\eta)=0,\\ \varphi'(\eta)=K_2\varphi(\eta),\ \ \delta l'(\eta)=-K_2\varphi(\eta)\quad \text{at } \eta=0\\ f'(\infty)=0,\ \ f''(\infty)=0,\ \ \theta(\infty)=1,\ \ \varphi(\infty)=1, l(\infty)=0.\end{array}\right\}. \tag{16}$$

In above expression, the dimensionless parameters are $M=\frac{\sigma_f B_0^2}{a\rho_f}$, $\beta=\frac{\alpha_1^* a}{\mu_f}$, $K=\sqrt{\frac{a}{\nu_f}}R$, $Rd=\frac{16\sigma^* T_\infty^3}{3k^* k_f}$, $Nb=\frac{\tau D_B C_0}{\nu_f}$, $Me=\frac{(c_p)_f(T_\infty-T_m)}{\lambda+C_s(T_m-T_0)}$, $Nt=\frac{\tau D_T(T_\infty-T_m)}{T_\infty \nu_f}$, $Ec=\frac{u_w^2}{c_p(T_\infty-T_m)}$, $\mathrm{Pr}=\frac{\nu_f}{\alpha}$, $Q=\frac{Q_0}{a(\rho c_p)_f}$, $Sc=\frac{\nu_f}{D_{C_1}}$, $\delta=\frac{D_{C_2}}{D_{C_1}}$, $K_1=\frac{k_1^* C_0^2}{a}$, and $K_2=\frac{k_2^*}{D_{C_1}}\sqrt{\frac{a}{\nu_f}}$.

By neglecting the pressure we get

$$\left.\begin{array}{l}f^{iv}+\frac{2}{(\eta+K)}f'''-\frac{1}{(\eta+K)^2}f''+\frac{1}{(\eta+K)^3}f'+\frac{K}{(\eta+K)}\left(ff'''-f'f''\right)+\frac{K}{(\eta+K)^2}\left(ff''-f'^2\right)-\frac{K}{(\eta+K)^3}ff'\\ +2\beta\left(\begin{array}{l}\frac{K}{(\eta+K)}f''f'''+\frac{K}{(\eta+K)}f'f^{iv}+\frac{3K}{(\eta+K)^3}ff'''-\frac{5K}{(\eta+K)^2}f'f'''-\frac{K}{(\eta+K)^2}ff^{iv}\\ +\frac{12K}{(\eta+K)^3}f'f''-\frac{4K}{(\eta+K)^2}f''^2-\frac{6K}{(\eta+K)^4}ff''-\frac{8K}{(\eta+K)^4}f'^2+\frac{6K}{(\eta+K)^5}ff'\end{array}\right)\\ -M\left(f''+\frac{1}{(\eta+K)}f'\right)=0\end{array}\right\}. \tag{17}$$

Consider we have $D_{C_1}=D_{C_2}$ we have

$$\varphi(\eta)+l(\eta)=1$$

From equations (14) and (15) we have

$$\frac{1}{Sc}\left(\varphi''+\frac{1}{(\eta+K)}\varphi'\right)+\frac{K}{(\eta+K)}f\varphi'+\frac{1}{Sc}\frac{Nt}{Nb}\left(\theta''+\frac{1}{(\eta+K)}\theta'\right)-K_1\varphi(1-\varphi)^2=0 \tag{18}$$

$$\varphi'(\eta) = K_2\varphi(\eta), \quad \varphi(\infty) = 1. \tag{19}$$

Physical quantities

Skin friction coefficient

Mathematically

$$C_{fs} = \frac{\tau_{rs}}{\frac{1}{2}\rho_f u_w^2}, \tag{20}$$

shear stress (τ_{rs}) is given as

$$\tau_{rs} = \mu_f\left(\frac{\partial u}{\partial r} - \frac{u}{r+R}\right) + 2\alpha\left(\frac{R}{r+R}\frac{\partial u}{\partial r}\frac{\partial u}{\partial s} + \frac{v}{r+R}\frac{\partial u}{\partial r} - \frac{2Ru}{(r+R)^2}\frac{\partial u}{\partial s} - \frac{2uv}{(r+R)^2}\right)\Bigg|_{r=0}, \tag{21}$$

One can found

$$C_{fs}Re_s^{1/2} = 2\left[f''(0) - \frac{f'(0)}{K} + \beta\left(f'(0)f''(0) - \frac{2}{K}\left(f'(0)^2\right)\right)\right]. \tag{22}$$

Heat transfer rate

It is expressed as

$$Nu_s = \frac{sq_w}{k_f(T_\infty - T_m)} \tag{23}$$

Here q_w heat flux is defined as

$$q_w = -k_f\left(1 + \frac{16\sigma^* T_\infty^3}{3k^* k_f}\right)\frac{\partial T}{\partial r} \tag{24}$$

We get

$$Nu_sRe_s^{-1/2} = -(1 + Rd)\theta'(0). \tag{25}$$

Entropy modeling

It is expressed as

$$S_G = \left.\begin{matrix} \dfrac{k_f}{T_\infty^2}\left(1 + \dfrac{16\sigma^* T_\infty^3}{3k^* k_f}\right)\left(\dfrac{\partial T}{\partial r}\right)^2 + \dfrac{\sigma_f B_0^2}{T_\infty}u^2 + \dfrac{RD_{C_1}}{T_\infty}\left(\dfrac{\partial T}{\partial r}\dfrac{\partial C_1}{\partial r}\right) + \dfrac{RD_{C_1}}{C_1}\left(\dfrac{\partial C_1}{\partial r}\right)^2 \\ \dfrac{RD_{C_2}}{T_\infty}\left(\dfrac{\partial T}{\partial r}\dfrac{\partial C_2}{\partial r}\right) + \dfrac{RD_{C_2}}{C_2}\left(\dfrac{\partial C_2}{\partial r}\right)^2 \end{matrix}\right\}, \tag{26}$$

One can write

$$N_G(\eta) = \alpha_{11}(1+Rd)\theta'^2 + MBrf'^2 + \frac{\varphi'^2}{\alpha_1}\left(\frac{L_1}{\phi} + \frac{L_2}{(1-\phi)}\right) + (L_1 - L_2)\theta'\varphi'. \tag{27}$$

Here dimensionless variables are $S_G = \frac{S_G T_\infty \nu_f}{ak_f(T_\infty - T_m)}$, $Br = \frac{\mu_f u_w^2}{k_f(T_\infty - T_m)}$, $L_1 = \frac{RD_{C_2}C_0}{k_f}$, $\alpha_1 = \frac{T_\infty - T_m}{T_\infty}$, and $L_2 = \frac{RD_{C_2}C_0}{k_f}$.

Solution methodology

Optimal homotopic analysis method (OHAM) is employed to develop convergent solution.[46,47] Here, linear operators and initial approximation are defined as

$$\left.\begin{aligned} f_0(\eta) &= \left(e^{-\eta} - e^{-2\eta}\right) - \frac{Me}{\Pr} \\ \theta_0(\eta) &= 1 - e^{-\eta} \\ \varphi_0(\eta) &= 1 - e^{-K_2\eta} \end{aligned}\right\} \tag{28}$$

$$\left.\begin{aligned} L_f &= \frac{\partial^4}{\partial\eta^4} - 5\frac{\partial^2}{\partial\eta^2} + 4 \\ L_\theta &= \frac{\partial^2}{\partial\eta^2} - 1 \\ L_\varphi &= \frac{\partial^2}{\partial\eta^2} - 1 \end{aligned}\right\} \tag{29}$$

with

$$\left.\begin{matrix} L_f\left[c_1e^{\eta} + c_2e^{-\eta} + c_3e^{2\eta} + c_4e^{-2\eta}\right], \quad L_\theta[c_5e^{\eta} + c_6e^{-\eta}] \\ L_\varphi[c_7e^{\eta} + c_8e^{-\eta}] \end{matrix}\right\} \tag{30}$$

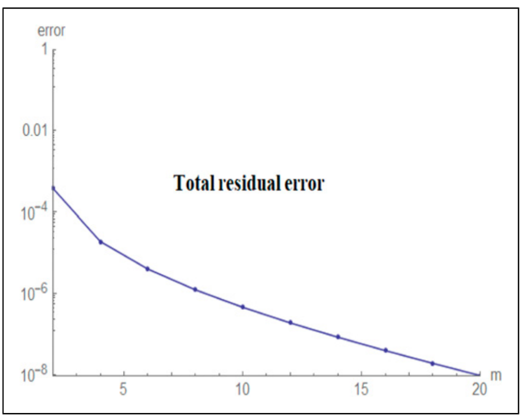

Figure 2. Total residual error.

Table 1. Total residual error for the velocity, temperature and concentration.

m	ε_m^f	ε_m^θ	ε_m^φ
2	0.000221245	0.0000635364	0.0000866985
4	3.35461×10^{-7}	1.01235×10^{-9}	0.00001512547
8	1.47896×10^{-10}	1.5421×10^{-11}	1.12451×10^{-7}
12	1.14532×10^{-13}	1.3654×10^{-14}	1.36542×10^{-8}
16	1.45632×10^{-16}	3.67895×10^{-17}	3.78654×10^{-9}
20	1.56421×10^{-19}	1.54213×10^{-19}	5.12452×10^{-10}

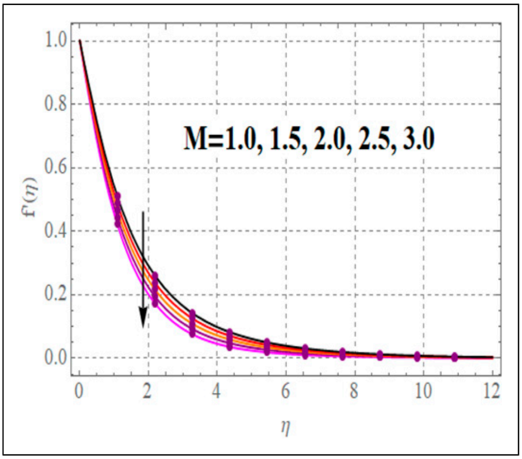

Figure 3. $f'(\eta)$ versus M.

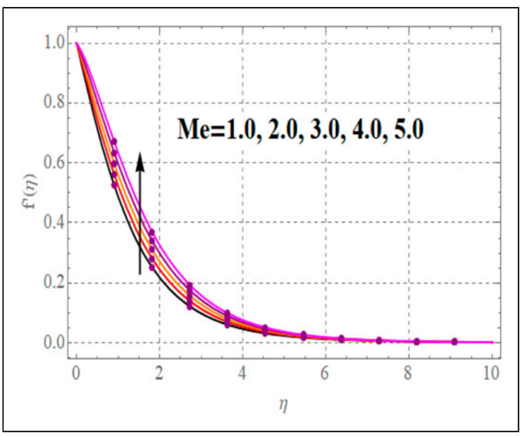

Figure 4. $f'(\eta)$ versus Me.

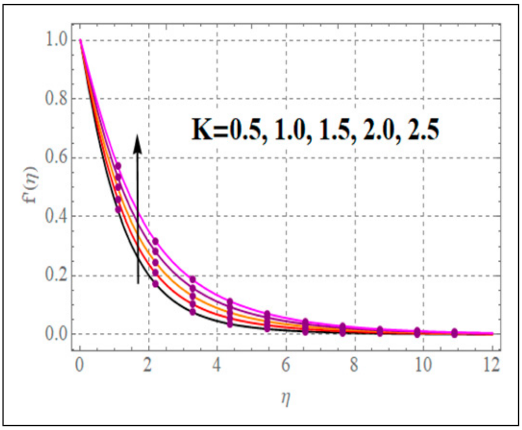

Figure 5. $f'(\eta)$ versus K.

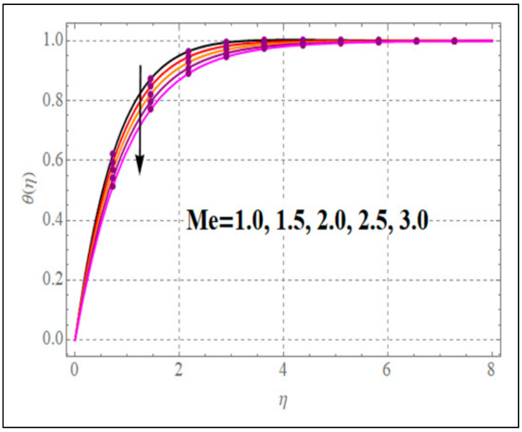

Figure 6. $\theta(\eta)$ versus Me.

Here, c_i $(i = 1, 2,...,8)$ denotes the arbitrary constants.

Convergence Analysis

Initially, Liao [46,47] gives the concept of optimal homotopic analysis technique. Mathematically it is expressed as

$$\varepsilon_m^f = \frac{1}{k+1} \sum_{i=0}^{k} \left[\aleph_f \left(\sum_{j=0}^{m} f(\eta) \right)_{\eta = i\delta^* \eta} \right]^2, \tag{31}$$

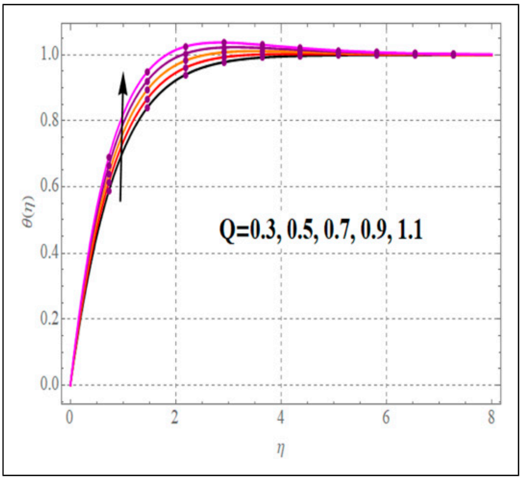

Figure 7. $\theta(\eta)$ versus *Q*.

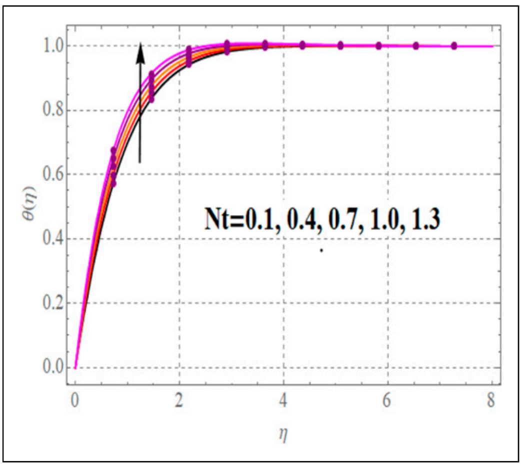

Figure 8. $\theta(\eta)$ versus *Nt*.

$$\varepsilon_m^{\theta} = \frac{1}{k+1}\sum_{i=0}^{k}\left[\aleph_{\theta}\left(\sum_{j=0}^{m} f(\eta), \sum_{j=0}^{m}\theta(\eta)\right)_{\eta=i\delta^{*}\eta}\right]^2, \tag{32}$$

$$\varepsilon_m^{\varphi} = \frac{1}{k+1}\sum_{i=0}^{k}\left[\aleph_{\varphi}\left(\sum_{j=0}^{m} f(\eta), \sum_{j=0}^{m}\theta(\eta), \sum_{j=0}^{m}\varphi(\eta)\right)_{\eta=i\delta^{*}\eta}\right]^2, \tag{33}$$

Total squared residual error is [46,47]

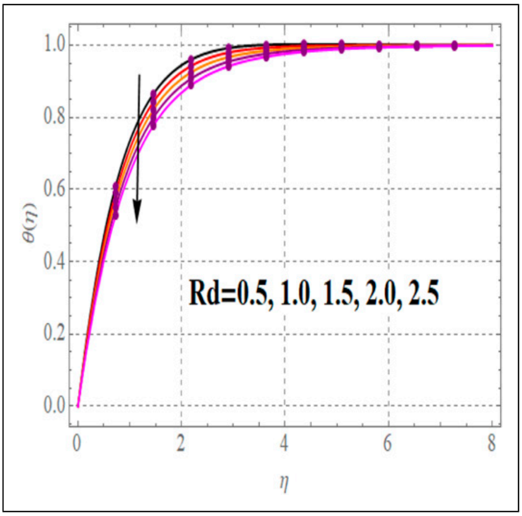

Figure 9. $\theta(\eta)$ versus *Rd*.

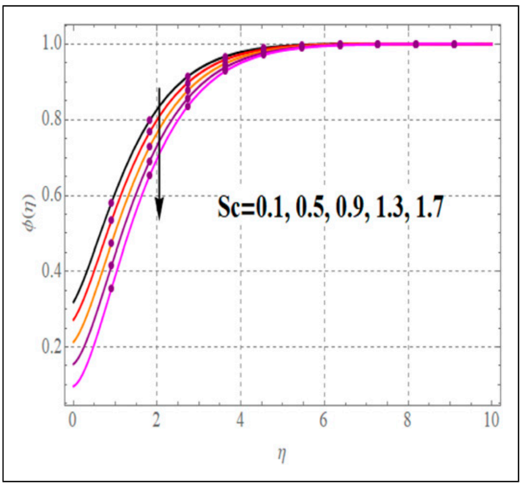

Figure 10. $\varphi(\eta)$ versus *Sc*.

$$\varepsilon_m^t = \varepsilon_m^f + \varepsilon_m^\theta + \varepsilon_m^\varphi.$$

Figure 2 shows the total averaged squared residual error.
Individual averaged residual errors are highlighted in Table 1.

Graphical results and analysis

Significant performance of fluid flow, entropy rate, thermal field, and concentration against physical variable are studied.

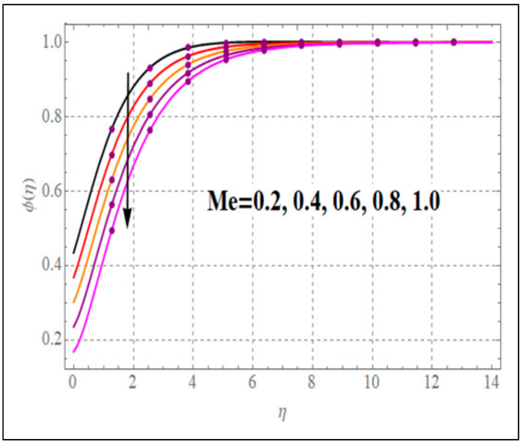

Figure 11. $\varphi(\eta)$ versus *Me*.

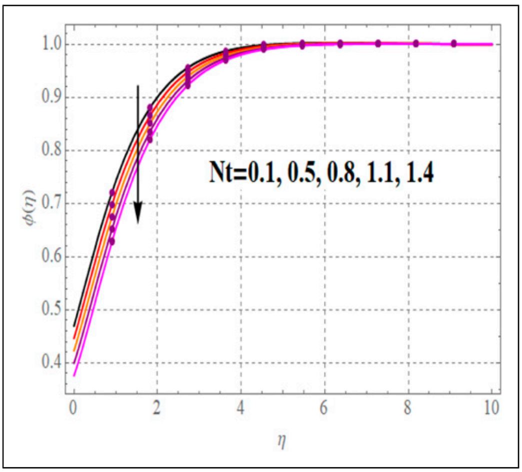

Figure 12. $\varphi(\eta)$ versus *Nb*.

Velocity

Performance of fluid flow against magnetic variable is portrayed in Figure 3. An amplification in magnetic effect improves the resistive force which reduced the fluid flow. Influence of melting effect on velocity $(f'(\eta))$ is exhibited in Figure 4. Higher estimation of melting parameter corresponds to rises velocity $(f'(\eta))$. Significant effect of velocity versus curvature variable is shown in Figure 5. An intensification in curvature variable (K) reduces the viscous force and as a result fluid flow is boosted.

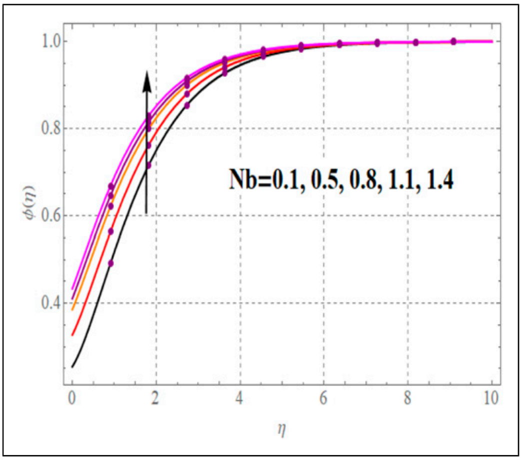

Figure 13. $\varphi(\eta)$ versus *Nt*.

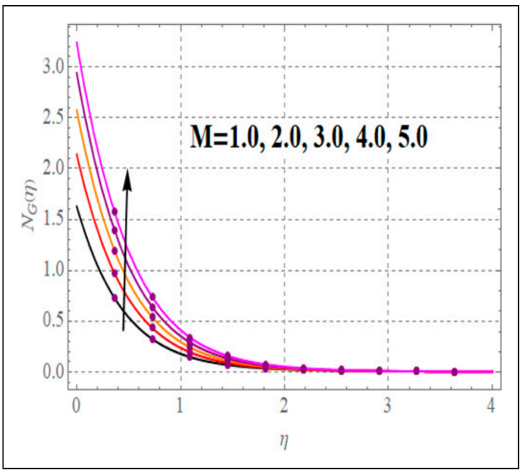

Figure 14. $N_G(\eta)$ versus *M*.

Temperature

Influence of thermal field via melting variable is depicted in Figure 6. Larger approximation in melting (Me) variable declines the temperature $(\theta(\eta))$ distribution. Heat generation variable impact on thermal field is illustrated in Figure 7. An augmentation in temperature is noticed through heat generation (Q) variable. An increasing behavior in thermal field is noted with variation in thermophoretic variable (see Figure 8). Outcomes of radiation on thermal field $(\theta(\eta))$ are illustrated in Figure 9. Here, one can found that temperature boosts up with higher radiation effect.

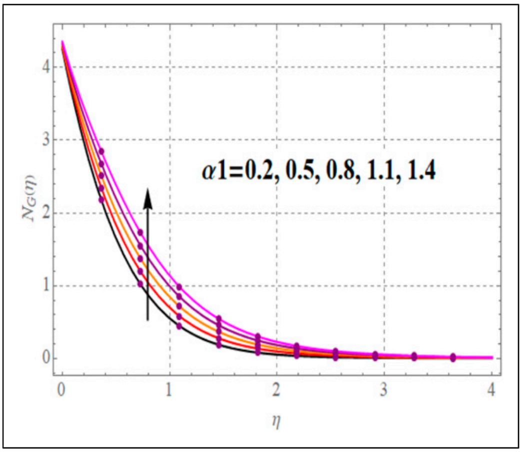

Figure 15. $N_G(\eta)$ versus $\alpha 1$.

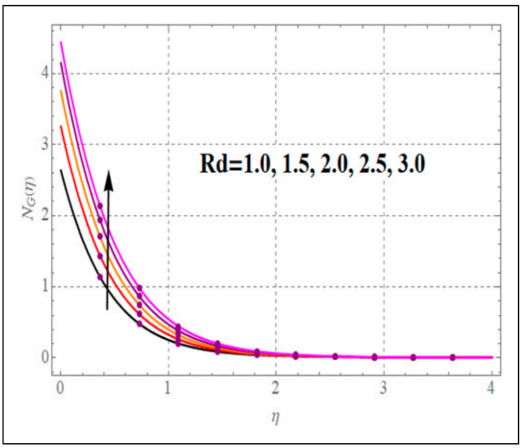

Figure 16. $N_G(\eta)$ versus Rd.

Concentration

Outcome of concentration with higher Schmidt number is depicted in Figure 10. A decrement in mass diffusivity is noticed with rising Schmidt number, which decreases concentration. Reduction occurs in concentration with variation in melting variable (see Figure 11). Influence of random and thermophoretic motion variables on concentration is revealed in Figures 12 and 13. Clearly reverse trend holds for concentration through thermophoretic and random motion variables.

Entropy rate

Figure 14 elucidates influence of entropy rate against magnetic variable. An intensification in magnetic effect improves the resistive force between liquid particles, which enhances the disorderness in thermal system. As a result, entropy rate boosted. An increment in thermal ratio variable $(\alpha 1)$ enhances the entropy rate (see Figure 15). Figure 16 shows outcome of radiation on entropy generation $(N_G(\eta))$. A decrement in coefficient of mean absorption with higher radiation, which rises thermal emission and thus entropy generation, is augmented.

Conclusions

The key findings are given below.

- An amplification in fluid flow is observed through curvature variable, while opposite impact holds for magnetic variable.
- An opposite behavior holds for fluid flow and thermal field through melting variable.
- Thermal field increased with variation in heat generation variable.
- Larger estimation of radiation boosts up entropy rate, while opposite impact holds for thermal field.
- An opposite impact in concentration is noticed through random and thermophoretic variable.
- A decrement in concentration is seen through Schmidt number.
- An intensification in thermal field is seen through magnetic variable.

Acknowledgment

The Deanship of Scientific Research (DSR) at King Abdulaziz University (KAU), Jeddah, Saudi Arabia has funded this project under grant no (G: 328-130-1443).

Declaration of conflicting interests

The author(s) declared no potential conflicts of interest with respect to the research, authorship, and/or publication of this article.

References

1. Roberts L. On the melting of a semi-infinite body of ice placed in a hot stream of air. *J Fluid Mech* 1958; 4: 505–528.
2. Hayat T, Muhammad K, Alsaedi A, et al. Thermodynamics by melting in flow of an Oldroyd-B material. *J Braz Soc Mech Sci Eng* 2018; 40, DOI: 10.1007/s40430-018-1447-3.
3. Das K. Radiation and melting effects on MHD boundary layer flow over a moving surface. *Ain Shams Eng J* 2014; 5: 1207–1214.
4. Hayat T, Khan SA, Khan MI, et al. Optimizing the theoretical analysis of entropy generation in flow of second grade nanofluid. *Physica Scripta* 2019; 94: 085001.
5. Waqas M, Khan MI, Hayat T, et al. Transportation of radiative energy in viscoelastic nanofluid considering buoyancy forces and convective conditions, Chaos. *Solitons & Fractals* 2020; 130: 109415.
6. Mally N and Haussener S. Buoyancy-driven melting and solidification heat transfer analysis in encapsulated phase change materials. *Int J Heat Mass Trans* 2021; 164: 120525. DOI: 10.1016/j.ijheatmasstransfer.2020.120525.
7. Hayat T, Shah F, Alsaedi A, et al. Entropy optimized dissipative flow of effective Prandtl number with melting heat transport and Joule heating. *Int Communi Heat Mass Trans* 2020; 111: 10444. DOI: 10.1016/j.icheatmasstransfer.2019.104454.

8. Qi R, Wang Z, Ren J, et al. Numerical investigation on heat transfer characteristics during melting of lauric acid in a slender rectangular cavity with flow boundary condition. *Int J Heat Mass Trans* 2020; 157: 119927. DOI: 10.1016/j.ijheatmasstransfer.2020.119927.
9. Farahani SD, Farahani AD, Tayebzadeh F, et al. Melting of non-Newtonian phase change material in a finned triple-tube: efficacy of non-uniform magnetic field. *Case Stud Therm Eng* 2021; 28: 101543. DOI: 10.1016/j.csite.2021.101543.
10. Wang H, Xu H, Liu C, et al. Numerical investigation of melting enhancement for paraffin in an innovative finned-plate latent heat thermal energy storage unit. *J Energy Storage* 2021; 43: 103222. DOI: 10.1016/j.est.2021.103222.
11. Choi SUS. Enhancing thermal conductivity of fluids with nanoparticles. *ASME-Publications-Fed* 1995; 231: 99–106.
12. Eastman JA, Choi SUS, Li S, et al. Anomalously increased effective thermal conductivities of ethylene glycol-based nanofluids containing copper nanoparticles. *App Phy Lett* 2001; 78: 718–720.
13. Bhanvase B and Barai D. Heat transfer using nanofluids. *Nanofluids Heat Mass Transf* 2021: 281–336.
14. Saidur R, Leong KY and Mohammed HA. A review on applications and challenges of nanofluids. *Renew Sustain Energy Rev* 2011; 15: 1646–1668.
15. Buongiorno J. Convective transport in nanofluids. *J Heat Trans* 2006; 128: 240–250.
16. Urmi WT, Rahman MM, Kadirgama K, et al. An overview on synthesis, stability, opportunities and challenges of nanofluid. *Materialstoday: Proc* 2021; 41: 30–37.
17. Reddy MG and Makinde OD. Magnetohydrodynamic peristaltic transport of Jeffrey nanofluid in an asymmetric channel. *J Mol Liq* 2016; 223: 1242–1248.
18. Hayat T, Inayat U, Momani S, et al. FDM analysis for nonlinear mixed convective nanofluid flow with entropy generation. *Int Comm Heat Mass Transf* 2021; 126: 105389.
19. Hayat T, Khan SA and Alsaedi A. Entropy analysis for second grade nanomaterials flow with thermophoresis and Brownian diffusions. *Int Communi Heat Mass Trans* 2021; 127: 105564. DOI: 10.1016/j.icheatmasstransfer.2021.105564.
20. Mabood F, Shamshuddin M and Mishra SR. Characteristics of thermophoresis and Brownian motion on radiative reactive micropolar fluid flow towards continuously moving flat plate: HAM solution. *Math Comput Simul* 2022; 191: 187–202.
21. Ahmad S, Ahmad A, Ali K, et al. Effect of non-Newtonian flow due to thermally-dependent properties over an inclined surface in the presence of chemical reaction, Brownian motion and thermophoresis. *Alex Eng J* 2021; 60: 4931–4945.
22. Hayat T, Tamoor M, Khan MI, et al. Numerical simulation for nonlinear radiative flow by convective cylinder. *Results Phys* 2016; 6: 1031–1035.
23. Farooq M, Anjum A and Masood S. Dissipative effects in hydromagnetic nanomaterial flow with variable fluid characteristics: Modern diffusion analysis. *Int Communi Heat Mass Trans* 2021; 127: 105503. DOI: 10.1016/j.icheatmasstransfer.2021.105503.
24. Gowda RJP, Kumar RN, Prasannakumara BC, et al. Exploring magnetic dipole contribution on ferromagnetic nanofluid flow over a stretching sheet: An application of Stefan blowing. *J Mol Liq* 2021; 335: 116215. DOI: 10.1016/j.molliq.2021.116215.
25. Harish R and Sivakumar R. Effects of nanoparticle dispersion on turbulent mixed convection flows in cubical enclosure considering Brownian motion and thermophoresis. *Powder Technol* 2021; 378: 303–316.
26. Bejan A. Second law analysis in heat transfer. *Energy* 1980; 5: 721–732.
27. Bejan A. Entropy generation minimization: The new thermodynamics of finite-size devices and finite-time processes. *J App Phy* 1996; 79: 1191–1218. DOI: 10.1063/1.362674.

28. Kumar A, Tripathi R, Singh R, et al. Simultaneous effects of nonlinear thermal radiation and Joule heating on the flow of Williamson nanofluid with entropy generation. *Phy A Statist Mech Appli* 2020; 551: 123912. DOI: 10.1016/j.physa.2019.123972.
29. Hassan AR. The entropy generation analysis of a reactive hydromagnetic couple stress fluid flow through a saturated porous channel. *App Math Compu* 2020; 369: 124843. DOI: 10.1016/j.amc.2019.124843.
30. Hayat T, Khan SA, Khan MI, et al. Theoretical investigation of Ree--Eyring nanofluid flow with entropy optimization and Arrhenius activation energy between two rotating disks. *Comp Meth Program Biomed* 2019; 177: 57–68.
31. Khan MI, Alsaedi A, Hayat T, et al. Modeling and computational analysis of hybrid class nanomaterials subject to entropy generation. *Computer Methods Programs Biomed* 2019; 179: 104973.
32. Zhang Z, Lou C, Li Z, et al. Evaluation of radiative entropy generation in a high temperature system including H2O, CO2 and soot with non-gray wall. *J Quant Spectrosc Radiat Trans* 2020; 253: 107175. DOI: 10.1016/j.jqsrt.2020.107175.
33. Shahsavar A, Rashidi M, Yldz Ç, et al. Natural convection and entropy generation of Ag-water nanofluid in a finned horizontal annulus: A particular focus on the impact of fin numbers. *Int Communi Heat Mass Trans* 2021; 125: 105349. DOI: 10.1016/j.icheatmasstransfer.2021.105349.
34. Farooq U, Waqas H, Imran M, et al. On melting heat transport and nanofluid in a nozzle of liquid rocket engine with entropy generation. *J Mater Res Technol* 2021; 14: 3059–3069.
35. Priam SS and Nasrin R. Oriented magneto-conjugate heat transfer and entropy generation in an inclined domain having wavy partition. *Int Communi Heat Mass Trans* 2021; 126: 105430. DOI: 10.1016/j.icheatmasstransfer.2021.105430.
36. Torabi M, Karimi N, Torabi M, et al. Generation of entropy in micro thermofluidic and thermochemical energy systems-A critical review. *Int J Heat Mass Trans* 2020; 163: 120471. DOI: 10.1016/j.ijheatmasstransfer.2020.120471.
37. Qayyum S, Khan MI, Hayat T, et al. Comparative investigation of five nanoparticles in flow of viscous fluid with Joule heating and slip due to rotating disk. *Physica B: Condensed Matter* 2018; 534: 173–183.
38. Wu Y, Peng Q, Yang M, et al. Entropy generation analysis of premixed hydrogen--air combustion in a micro combustor with porous medium. *Chem Eng Process* 2021; 168: 108566. DOI: 10.1016/j.cep.2021.108566.
39. Hayat T, Qayyum S, Alsaedi A, et al. Darcy-Forchheimer nanofluid flow due to curved stretching sheet with partial slip. *Int Communi Heat Mass Trans* 2020; 111: 104445. DOI: 10.1016/j.icheatmasstransfer.2019.104445.
40. Sakly A and Nejma FB. Heat and mass transfer of combined forced convection and thermal radiation within a channel: entropy generation analysis. *App Ther Eng* 2020; 171: 114903. DOI: 10.1016/j.applthermaleng.2020.114903.
41. Liao SJ. *Homotopy analysis method in nonlinear differential equations*. Heidelberg, Germany: Springer, 2012.
42. Liao S. An optimal homotopy-analysis approach for strongly nonlinear differential equations. *Communi Nonlinear Sci Numer Simul* 2010; 15: 2003–2016.
43. Hayat T, Shafiq A and Alsaedi A. Characteristics of magnetic field and melting heat transfer in stagnation point flow of Tangent-hyperbolic liquid. *J Magn Mag Mater* 2016; 405: 97–106.
44. Sheikholeslami M, Hatami M and Ganji DD. Micropolar fluid flow and heat transfer in a permeable channel using analytical method. *J Mol Liq* 2014; 194: 30–36.
45. Han S, Zheng L, Li C, et al. Coupled flow and heat transfer in viscoelastic fluid with Cattaneo--Christov heat flux model. *App Math Lett* 2014; 38: 87–93.
46. Animasaun IL, Mahanthesh B, Sarojamma G, et al. Significance of thickness of paraboloid of revolution and buoyancy forces on the dynamics of Erying--Powell fluid subject to equal diffusivity kind of quartic autocatalysis. *Phy A* 2020; 549: 124047. DOI: 10.1016/j.physa.2019.124047.

47. Kumar R, Kumar R, Sheikholeslami M, et al. Irreversibility analysis of the three dimensional flow of carbon nanotubes due to nonlinear thermal radiation and quartic chemical reactions. *J Mol Liq* 2019; 274: 379–392.
48. Makinde OD and Animasaun IL. Thermophoresis and Brownian motion effects on MHD bioconvection of nanofluid with nonlinear thermal radiation and quartic chemical reaction past an upper horizontal surface of a paraboloid of revolution. *J Mol Liq* 2016; 221: 733–743.
49. Animasaun IL. 47nm alumina--water nanofluid flow within boundary layer formed on upper horizontal surface of paraboloid of revolution in the presence of quartic autocatalysis chemical reaction. *Alex Eng J* 2016; 55: 2375–2389.
50. Saif RS, Muhammad T, Sadia H, et al. Hydromagnetic flow of Jeffrey nanofluid due to a curved stretching surface. *Phy A* 2020; 551: 124060. DOI: 10.1016/j.physa.2019.124060.
51. Khan MI and Alzahrani F. Nonlinear dissipative slip flow of Jeffrey nanomaterial towards a curved surface with entropy generation and activation energy. *Mathem Compu Simul* 2021; 185: 47–61.
52. Hayat T, Shah F and Alseadi A. Cattaneo-Christov double diffusions and entropy generation in MHD second grade nanofluid flow by a Riga wall. *Int Communi Heat Mass Trans* 2020; 119: 104824. DOI: 10.1016/j.icheatmasstransfer.2020.104824.

Appendix

Nomenclature

A, B	chemical species Me melting parameter
C_0	ambient concentration Ec Eckert number
C_1	homogeneous concentration Nt thermophoresis parameter
C_2	heterogeneous concentration Nb Brownian motion parameter
c_p	specific heat N_G entropy generation
D_{C_1}, D_{C_2}	diffusion coefficients L_1 homogeneous diffusion parameter
D_T	thermophoresis coefficient L_2 heterogeneous diffusion parameter
k^*	mean absorption coefficient α_1 temperature difference parameter
k_f	thermal conductivity Re_s local Reynold number
k_1^*	reaction rate (homogeneous species) Sc Schmidt number
k_2^*	reaction rate (heterogeneous species) K_1 homogeneous reaction parameter
p	pressure K_2 heterogeneous reaction parameter
Q_0	heat generation coefficient R molar gas constant
r, s	curvilinear coordinates β fluid parameter
T	temperature M magnetic parameter
T_m	melting heat temperature Rd radiation parameter
T_∞	ambient temperature Pr Prandtl number
u, v	velocity components C_s surface heat capacity
α_1^*	material parameter δ diffusivity ratio
ρ_f	density C_{fs} surface drag force
ν_f	kinematic viscosity τ_{rs} shear stress
μ_f	dynamic viscosity Nu_s Nusselt number
σ_f	electrical conductivity q_w heat flux
σ^*	Stefan Boltzmann constant Br Brinkman number
λ	latent heat Q heat generation parameter